ACS APPLIED MATERIALS & INTERFACES

Research Article

www.acsami.org

# Printed Multilayer Microtaggants with Phase Change Nanoparticles for Enhanced Labeling Security

Binh Duong,[†,§] Helin Liu,[‡,§] Cheng Li,[‡] Weiwei Deng,[‡] Liyuan Ma,[†] and Ming Su*[,†,‡]

[†]Department of Biomedical Engineering, Worcester Polytechnic Institute, Worcester, Massachusetts 01609, United States

[‡]Department of Mechanical and Aerospace Engineering, University of Central Florida, Orlando, Florida 32826, United States

**ABSTRACT:** There is an urgent need to develop taggants that can be used to identify objects, prevent fraud, and deter counterfeiting with high reliability, high capacity, and minimal effort. This paper describes a new multilayer covert taggant based on phase change nanoparticles (metals and eutectic alloys). A panel of selected nanoparticles with different melting temperatures have been added in matrix materials together with fluorescent dye and printed on substrates to form micro-/macrofeatures that contain thermal, fluorescence signature, and structural components. The multilayer taggants can greatly enhance security level for many commercial and forensic applications by their extremely large labeling capacity, coding readiness, and covertness.

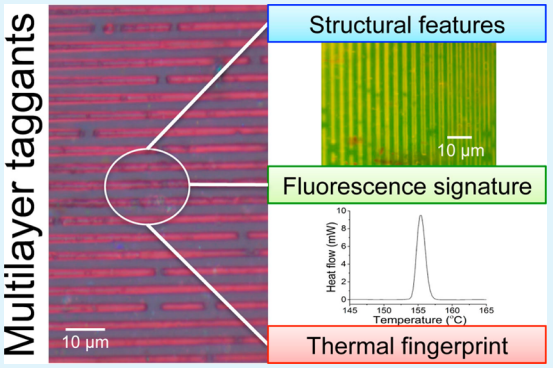


**KEYWORDS:** *printable taggants, multilayer microtaggants, phase change nanoparticles, authentication*

## 1. INTRODUCTION

Counterfeits generate serious issues for many industrial sections such as pharmaceuticals, airplane parts, auto parts, and clothing, etc. There are urgent commercial and forensic needs for a method that is capable of identifying product/materials, preventing fraud, or deterring counterfeits with high reliability and minimal effort. Although a variety of anticounterfeit technologies such as overt or visible features, covert or hidden markers, forensic techniques, and serialization have been developed, the use of a single approach cannot provide full protection against counterfeiting.[1] Bar codes printed on packages or color shifting inks/films or holograms are vulnerable to forgery because of their visibility and easiness to imitate, substitute, or adulterate. Optical bar codes depending on up-converting phosphors, fluorescence, and ultraviolet afterglow can be fabricated easily because of their low cost. At present, counterfeiters can copy most anti-counterfeiting technologies within 18 months.[2] One way to enhance the security level of labeling is to use multilayer taggants that contain fluorescent, microscopic features and numeric code sequence.[3] Such combination of multiple taggants with distinct signatures makes it very difficult to be replicated. Another way is to use covert taggant that can easily be incorporated into a multilayer taggants and can only be detectable with appropriate devices by properly trained personnel.

Covert taggants can be microscale texts or structures generated with state-of-the-art lithographic/synthetic techniques or imbedded holographic images.[4−6] But code information stored within these taggants may be lost if taggants are damaged. In addition, other covert markers[3] such as chemical taggants,[7,8] biological taggants,[9] DNA taggants,[10] and isotope ratios[11] are too sensitive to environment, will degrade over time, and can only function over a limited period of time. Ultrasmall nanoparticles with unique physical properties are promising as covert taggants for several reasons: (1) the small size of nanoparticles makes them invisible to naked eyes; (2) they can be added in many matrix materials without changing the property of the host; (3) a variety of properties such as optical, magnetic, electric, and electrochemical properties can be considered as possible means of readout; (4) nanoparticles or their liquid suspensions can be printed and stamped on objects as inks or ink additives. However, the use of nanoparticles to label each object within a large group has been seriously limited because of lack of nanoparticle-specific characters.

Solid materials can change to liquid phase at their melting temperatures. During the melting process, the temperature of the solid does not rise until it is completely molten. If the dimension of the solid is sufficiently small, the time it takes for phase transition can be negligible, and there is a sharp melting peak during the linear thermal scan in differential scanning calorimetry (DSC). Among many types of solid materials such as metallic materials, organic materials, ceramics, and salts, metals and alloys have large volumetric latent heats of fusion and are stable over a large temperature range. Metallic nanoparticles with single sharp melting peaks can be designed with phase diagram knowledge and made using colloid

**Received:** March 19, 2014
**Accepted:** May 14, 2014
**Published:** May 14, 2014

   dx.doi.org/10.1021/am501668x | *ACS Appl. Mater. Interfaces* 2014, 6, 8909−8912

synthesis techniques. If a panel of metallic nanoparticles with melting temperatures distributed over a large temperature range can be made, these nanoparticles can be distinguished from each other in a single thermal scan of DSC. The melting temperature and heat flow obtained from DSC thermogram will indicate the type and amount of nanoparticles, respectively. Furthermore, these nanoparticles can be added in matrix materials and printed or stamped onto other objects to form multilayer taggants.

This article describes a new multilayer taggant system based on phase change nanoparticles of metals and eutectic alloys, which can be added in matrix materials and printed on objects to form microscale features containing fluorescence and thermal signatures. The fluorescence additive will be used for initial screening. Microfeatures will add extra layer of protection, and phase change nanoparticles will be used for high capacity serialization or forensic investigation.

## 2. EXPERIMENTAL SECTION

All chemicals are reagent grade and used without purification. Indium, tin, bismuth, and their alloys powders are obtained from Sigma-Aldrich and used as received. Rhodamine 6G is obtained from Acros Organics and used as fluorescent dye. Polyureasilazane (Kion Defense Technologies, Inc.) and polyvinyl alcohol (PVA) (Sigma-Aldrich) are used as matrix materials. Rain-X is purchased from AutoZone and used as an antiadhesive agent. Dicumyl peroxide (Sigma-Aldrich) is used as a thermal initiator to lower the curing temperature of polyureasilazne.

Metallic and alloy nanoparticles are produced by nanoemulsion method. For instance, 0.2 g of bismuth powder is boiled in 40 mL of high boiling temperature fluid of poly-$\alpha$-olefin (PAO) at 300 °C for 3 h in nitrogen atmosphere. As the reaction time increases, the light yellow PAO becomes gray and dark gradually. The nanoparticles are harvested by centrifuge and washed by acetone to remove excess PAO. The metal nanoparticles have been characterized using a variety of techniques. Differential scanning calorimeter (PerkinElmer DSC7) is used to determine the thermal properties of nanoparticles, where 10 mg of nanoparticles is hermetically sealed in an aluminum pan and placed in DSC chamber with continuous nitrogen flow. Scanning electron microscope (SEM, JSM-7000F) operated at an accelerating voltage of 3 kV is used to characterize the morphology of nanoparticles.

## 3. RESULTS AND DISCUSSION

Multilayer taggants based on phase change nanoparticles will have larger coding capacity. Ten different metals that can form binary eutectic alloys among any two of them have been found from all metallic elements in the periodic table. The metals are aluminum, bismuth, cadmium, copper, gadolinium, indium, lead, magnesium, palladium, and silver. Some of these metals may be prone to oxidization, but thin oxide film around nanoparticle will not cause delay in melting because the thermal conductivity of oxide is much higher than that of air. According to the combination law of alloy formation, the metals can generate 10 types of metal nanoparticles, 45 types of binary eutectic alloy nanoparticles, 120 types of ternary eutectic alloy nanoparticles, 210 types of quaternary eutectic alloy nanoparticles, and so on. The total number of metals and eutectic alloys reaches 1023. Note the combination corresponding to no metal ($n$ is 0) should be removed. Fifty types of nanoparticles with distinct melting temperatures can be identified and used to form thermal bar codes, where the temperature differences between adjacent ones are 5 ± 0.2 °C. The total number of combinations will be $(2^{50} - 1)$ or $10^{15}$. The large number of combinations allows labeling of a huge number of products.

The eutectic compositions and according melting temperatures of alloys can be derived using Pandat 8.1 software. The software is built based on calculation of total Gibbs energy as a function of atomic ratio of elements in a system. At any given temperature, pressure, and composition, Gibbs free energy will be at the lowest when all phases reach thermodynamic equilibrium. Figure 1a and Figure 1b show DSC curves of

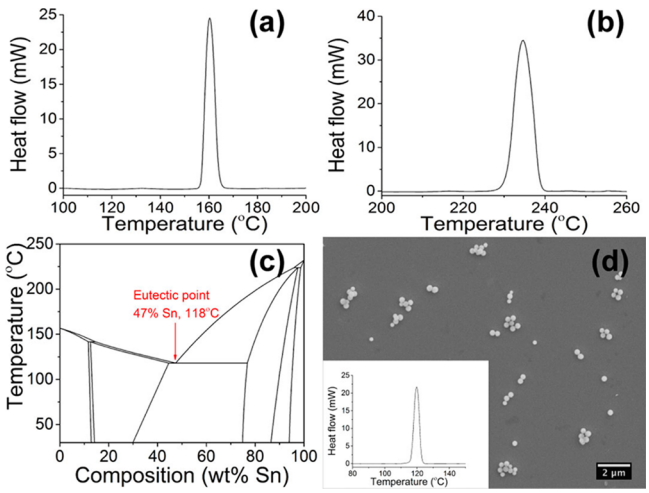


**Figure 1.** DSC curve of indium nanoparticles (a) and tin nanoparticles (b). Calculated indium−tin phase diagram (c). SEM image of indium−tin eutectic alloy nanoparticles (d) and according DSC curve (inset).

indium and tin nanoparticles with melting temperatures of 156 and 231 °C, respectively. The binary phase diagram of indium and tin has been obtained as shown in Figure 1c, where the eutectic composition and melting temperature are at 48% (tin) and 118 °C, respectively. The calculated eutectic composition is used to design eutectic alloys and synthesize alloy nanoparticles. SEM image (Figure 1d) shows that the average size of indium−tin eutectic alloy nanoparticles is 200 nm. Since the diameter of nanoparticles is larger than critical size (20 nm), the melting temperature is the same as their bulk counterparts.[12] The DSC curve of indium−tin nanoparticles shows a melting peak at 120 °C (Figure 1d inset), which is in good agreement with the calculated value (118 °C).

Multilayer taggants will allow multiple levels of identification. The visibility of graphic feature is intended to be used by customers or designated staff. The fluorescent characteristics is intended to be used for initial screening, and thermal bar code is aimed to be used by law enforcement or manufacture to determine whether a product is genuine. A 3D freestanding macroscale feature that contains fluorescent dye and six types of nanoparticles has been made by casting a mixture of 1 wt % rhodamine with nanoparticles of indium, tin, bismuth, and their alloys (indium−tin alloy, tin−bismuth alloy, indium−tin−bismuth alloy) in PVA matrix in a mold, followed by curing at 80 °C. Figure 2a and Figure 2b are optical image and fluorescent image of the feature. A small piece of this feature has been tested with DSC to examine its authenticity. Figure 2c shows the melting peaks of nanoparticles embedded in PVA matrix, where the DSC curve has been flattened to remove slope and smoothed to remove thermal fluctuation. The variation in peak height (or area) is due to the difference in amount of nanoparticles. The masses of phase change nanoparticles are 4.2 mg of indium−tin−bismuth alloy, 4.7

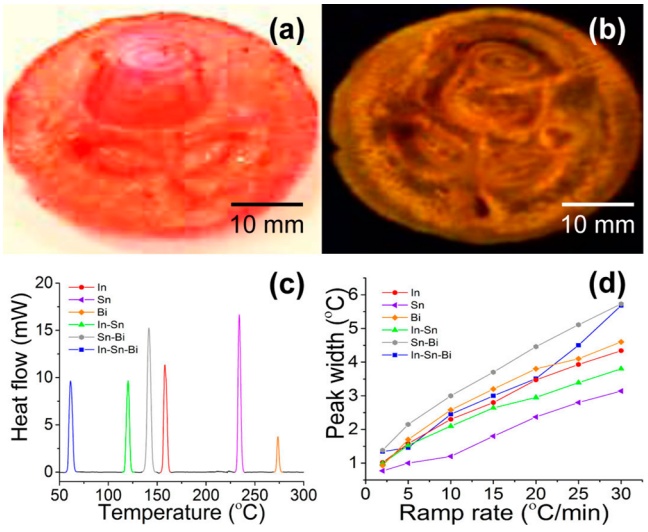


**Figure 2.** Optical image (a) and fluorescent image (b) of graphic logo with embedded fluorescence dye and phase change nanoparticles. DSC curve (c) and peak width (d) of six types of phase change nanoparticles embedded in the taggant.

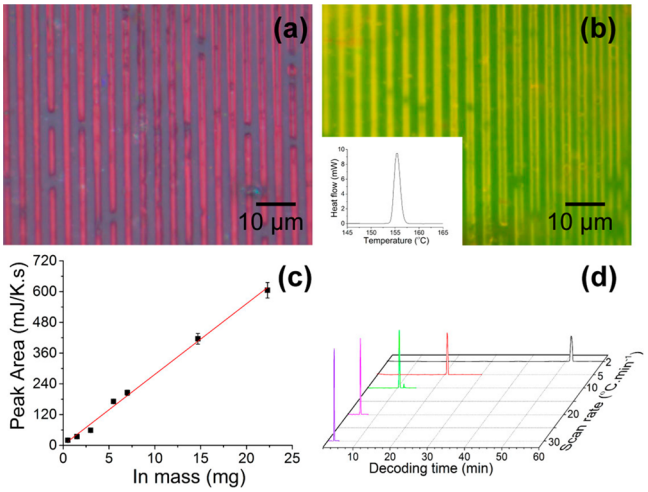


**Figure 3.** Optical image (a), fluorescent image (b), and thermal signature (b inset) of a multilayer taggant. Peak area calculated from the melting peak of indium nanoparticles at various mass loaded in the multilayer taggants (c). Decoding time of indium nanoparticles at different heating rates (d).

mg of indium−tin alloy, 8.9 mg of tin−bismuth alloy, 3.5 mg of indium, 5.3 mg of tin, and 1.6 mg of bismuth.

The spectral capacity of DSC depends on the width of the melting peak and thermal scan range. The scan range is determined by instrument and can go from room temperature up to thousands of degree. The width of melting peak in DSC can be derived from Gray's model[13,14] as

$$w = RC_s\left[\sqrt{1 + \frac{2\Delta H}{RC_s^2\beta}} - 1 + \ln 100\right]\beta \quad (1)$$

where $R$ is thermal resistance of whole system, $C_s$ is heat capacity of sample, $\Delta H$ is fusion enthalpy, $w$ is peak width at half height, and $\beta$ is the heating rate. The relationship between peak width of phase change nanoparticles and heating rate is shown in Figure 2d, where the peak width of metallic nanoparticles (i.e., metal and eutectic alloy) can be as small as 0.6 °C at a thermal ramp rate of 2 °C/min. Thus, it is possible to resolve 1000 melting peaks for a thermal scan in the range from 100 to 700 °C. The polymer matrix materials may decompose at high temperature, but that will not affect the applicability of this technique, as only a small amount of polymer−nanoparticles composite will be removed from the taggant and used for readout.

Nanoparticles (1% by weight) and rhodamine (1% by weight) are added in polyureasilazane (a preceramic polymer) and printed on solid substrate to form nonremovable multilayer taggant. To make micropatterns, a silicon master mold is first wetted with a commercial anti-adhesive agent (Rain-X), and the mixture is drop-casted onto a mold that is preheated at 200 °C. The printed structures are transferred onto a silicon substrate after curing for 30 s. Figure 3a and Figure 3b are the optical and fluorescence images of the printed microlines, respectively. Figure 3b inset is a DSC curve with melting peak at 156 °C, confirming the presence of indium nanoparticles. Figure 3c shows a linear relationship between peak area and the amount of indium nanoparticles, which is in good agreement with eq 2,

$$Q = mC_p\beta \quad (2)$$

where $Q$ is the heat flow (area of melting peak) and $m$, $C_p$, and $\beta$ are mass, specific heat of sample, and heating rate, respectively. The melting peak area can be obtained by integrating heat flow over melting range of nanoparticles. The minimum mass of indium nanoparticles in Figure 3c is 0.5 mg (which is limited by precision of balance), but the DSC machine is capable of detecting a much smaller amount of sample. The root-mean-square (rms) noise of the DSC (PerkinElmer 7) is 0.02 $\mu$W. The peak signal that can be recognized from background will be 0.02 $\mu$J for a 1 °C peak width at heating rate of 1 °C/s (60 °C/min). Given the latent heat of indium of 28 J/g, the lowest detectable mass of indium nanoparticle will be 1 ng. Even if any practically detectable signal should be 1000 times higher than noise, the detection limit for indium nanoparticles will be 1 $\mu$g. In addition, Figure 3d shows the relationship between decoding time and heating rate for indium nanoparticles, where decoding time can be shorter than 10 min when heating rate of 30 °C/min is used. According to eqs 1 and 2, operating at high heating rate will amplify the signal but peak width will increase. There are trade-offs and benefits of having a high operating rate for a particular application.

Multilayer taggant that contains phase change nanoparticles will have enhanced security level because it allows the brand owner to track and trace products even after the fluorescence tag loses its function because of photobleaching or the microstructure is destroyed because of physical damage. Three types of phase change nanoparticles and rhodamine dye have been added in PVA. The mixture is spin-coated over a silicon mold with microfeatures, cured at 150 °C, and then transferred onto thermal released tape to form removable taggant. Figure 4a shows an image of thus-produced PVA film attached on the tape, and fluorescent emission image under ultraviolet (365 nm) excitation can be used for initial screen (Figure 4a inset). Figure 4b is a SEM image of the printed structures, where the diameter and height of each feature are 8 and 5 $\mu$m, respectively. Although the microfeature is invisible to naked eyes, it can be verified by optical diffraction with a low-cost green laser pointer (Figure 4c), where the 2D periodic diffraction pattern represents the reciprocal spacing and


dx.doi.org/10.1021/am501668x | ACS Appl. Mater. Interfaces 2014, 6, 8909−8912

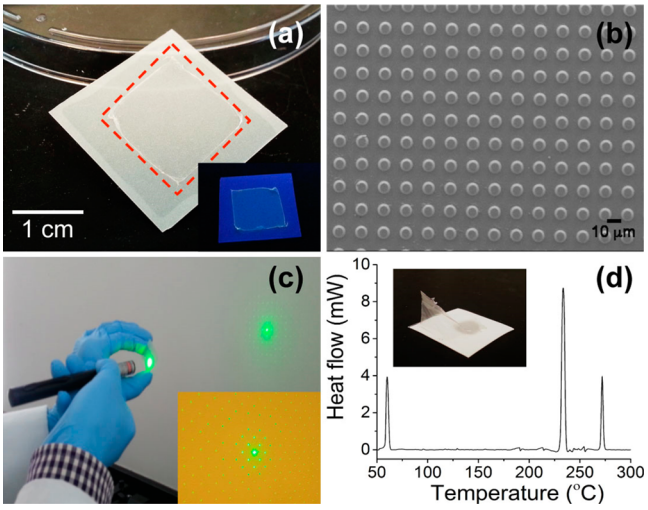


**Figure 4.** Photographs of multilayer taggants (red area) under white light (a) and under UV light (a inset). SEM image of microstructures on the pattern (b). Micropattern verified using laser pointer (c) as well as the diffraction pattern (c inset). DSC curve (d) of phase change nanoparticles (indium−tin−bismuth alloy, tin, and bismuth) of multilayer taggants after released from the tape (d inset).

orientation of the micrologo features on the film (Figure 4c inset). The film is then released from the tape by heating it over 90 °C, and the detached film (Figure 4d inset) is decoded with DSC. Figure 4d shows the presence of three types of nanoparticles, confirming the high reliability of thermal bar codes.

## 4. CONCLUSIONS

A new multilayer covert taggant system based on phase change nanoparticles has been created. Nanoparticles with sharp melting peaks and large latent heats of fusions are designed using phase diagram knowledge and prepared using colloid method. Selected panels of nanoparticles have been added into matrix materials together with fluorescence taggant and printed or patterned on substrate to form micro-/macroscale features that contain thermal and fluorescence signatures, as well as structural features. The use of multilayer taggants will greatly enhance labeling capacity for many commercial and forensic applications.

## AUTHOR INFORMATION

### Corresponding Author

* E-mail: msu2@wpi.edu.

### Author Contributions

§B.D. and H.L. contributed equally.

The manuscript was written through contributions of all authors. All authors have given approval to the final version of the manuscript.

### Notes

The authors declare no competing financial interest.

## ACKNOWLEDGMENTS

This project was supported by a New Investigator Award from National Institute of Justice (Grant 2012-DN-BX-K021) and a Faculty Early Career Development Award from National Science Foundations (Grant 1055599).

## REFERENCES

(1) Shah, R. Y.; Prajapati, P. N.; Agrawal, Y. K. Anticounterfeit Packaging Technologies. *J. Adv. Pharm. Technol. Res.* **2010**, *1*, 368−373.

(2) Deisingh, A. K. Pharmaceutical Counterfeiting. *Analyst* **2005**, *130*, 271−279.

(3) Braeckmans, K.; De Smedt, S. C.; Leblans, M.; Pauwels, R.; Demeester, J. Encoding Microcarriers: Present and Future Technologies. *Nat. Rev. Drug Discovery* **2002**, *1*, 447−456.

(4) Braeckmans, K.; De Smedt, S. C.; Roelant, C.; Leblans, M.; Pauwels, R.; Demeester, J. Encoding Microcarriers by Spatial Selective Photobleaching. *Nat. Mater.* **2003**, *2*, 169−173.

(5) Han, S.; Bae, H. J.; Kim, J.; Shin, S.; Choi, S. E.; Lee, S. H.; Kwon, S.; Park, W. Lithographically Encoded Polymer Microtaggant Using High-Capacity and Error-Correctable QR Code for Anti-Counterfeiting of Drugs. *Adv. Mater.* **2012**, *24*, 5924−5929.

(6) Huang, C. B.; Lucas, B.; Vervaet, C.; Braeckmans, K.; Van Calenbergh, S.; Karalic, I.; Vandewoestyne, M.; Deforce, D.; Demeester, J.; De Smedt, S. C. Unbreakable Codes in Electrospun Fibers: Digitally Encoded Polymers To Stop Medicine Counterfeiting. *Adv. Mater.* **2010**, *22*, 2657−2662.

(7) Kolla, P. The Application of Analytical Methods to the Detection of Hidden Explosives and Explosive Devices. *Angew. Chem., Int. Ed. Engl.* **1997**, *36*, 801−811.

(8) Czarnik, A. W. Encoding Methods for Combinatorial Chemistry. *Curr. Opin. Chem. Biol.* **1997**, *1*, 60−66.

(9) Kiel, J. L.; Holwitt, E. A.; Parker, J. E.; Vivkananda, J.; Franz, V.; Sloan, M. A.; Miziolek, A. W.; DeLucia, F. C.; Munson, C. A.; Mattley, Y. D. Specific Biological Agent Taggants. *Chemical and Biological Sensing*, Proceedings of SPIE, Orlando, FL, March 28−29, 2005; SPIE: Bellingham, WA, 2005.

(10) Clelland, C. T.; Risca, V.; Bancroft, C. Hiding Messages in DNA Microdots. *Nature* **1999**, *402*, 750−750.

(11) Geysen, H. M.; Wagner, C. D.; Bodnar, W. M.; Markworth, C. J.; Parke, G. J.; Schoenen, F. J.; Wagner, D. S.; Kinder, D. S. Isotope or Mass Encoding of Combinatorial Libraries. *Chem. Biol.* **1996**, *3*, 679−688.

(12) Jiang, H. J.; Moon, K. S.; Dong, H.; Hua, F.; Wong, C. P. Size-Dependent Melting Properties of Tin Nanoparticles. *Chem. Phys. Lett.* **2006**, *429*, 492−496.

(13) Gray, A. P. A Simple Generalized Theory for the Analysis of Dynamic Thermal Measurement. In *Analytical Calorimetry*; Porter, R. S., Johnson, J. F., Eds.; Plenum Press: New York, 1968; Vol. *1*, pp 209−219.

(14) Wang, G.; Harrison, I. R. Polymer Melting: Heating Rate Effects on DSC Melting. *Thermochim. Acta* **1994**, *231*, 203−213.